Electronic Supplementary Material (ESI) for Journal of Materials Chemistry C.

Supplementary Information

Ultrathin oxysulfide semiconductors from liquid metal: a wet chemical approach

Chung Kim Nguyen,[a] Mei Xian Low,[a] Ali Zavabeti,[b,c] Azmira Jannat,[a] Billy J Murdoch,[d] Enrico Della Gaspera,[b] Rebecca Orrell-Trigg,[b] Sumeet Walia,[a] Aaron Elbourne,[b] Vi Khanh Truong,[b] Chris F McConville,[b,e] Nitu Syed,*[a] Torben Daeneke*[a]

[a] School of Engineering, RMIT University, Melbourne, VIC 3001, Australia
[b] School of Science, RMIT University, Melbourne, VIC 3001, Australia
[c] Department of Chemical Engineering, The University of Melbourne, Parkville, VIC 3010, Australia
[d] RMIT Microscopy and Microanalysis Facility, College of Science, Engineering & Health, RMIT University, Melbourne, Victoria 3001, Australia
[e] Institute for Frontier Materials, Deakin University, Waurn Ponds, Geelong, VIC 3216, Australia

Email: nitu.syed@rmit.edu.au, torben.daeneke@rmit.edu.au

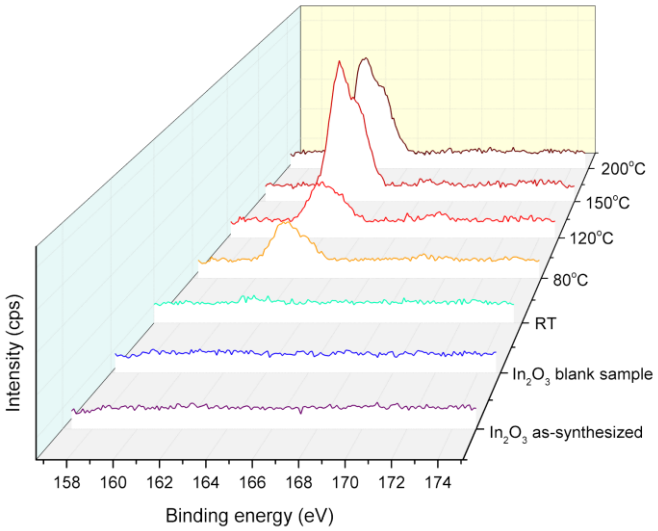

Figure S1. XPS spectra of S2*p* taken from samples treated at different temperatures in 5 hours. No signal was detected in the S2*p* regions of In_2O_3 as-synthesized, blank sample, and the sample treated at room temperature. The S2*p* peaks of S^{2-} are located at ~162 eV.[1]

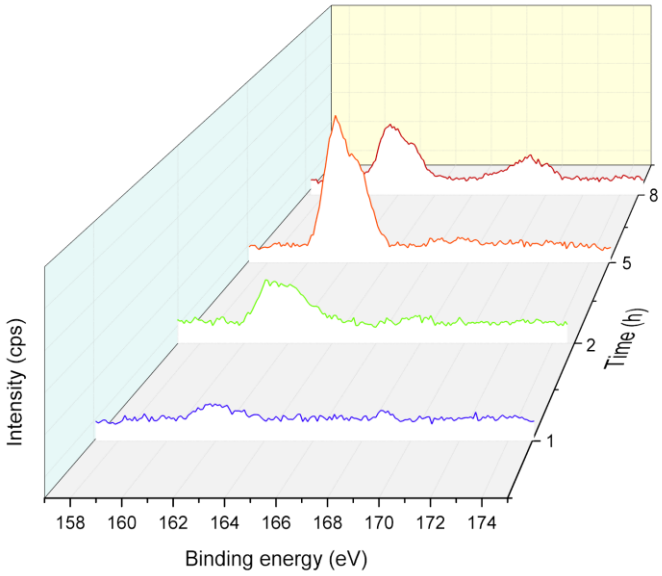

Figure S2. XPS spectra of S2*p* taken from samples treated at 150ºC after different reaction times. The S2*p* peaks of S^{2-} are located at ~162 eV, while the broaden peak at 169.1 eV detected in the sample after 8 hours is associated with sulfite/sulfate compounds (SO_4^{2-}).[1, 2]

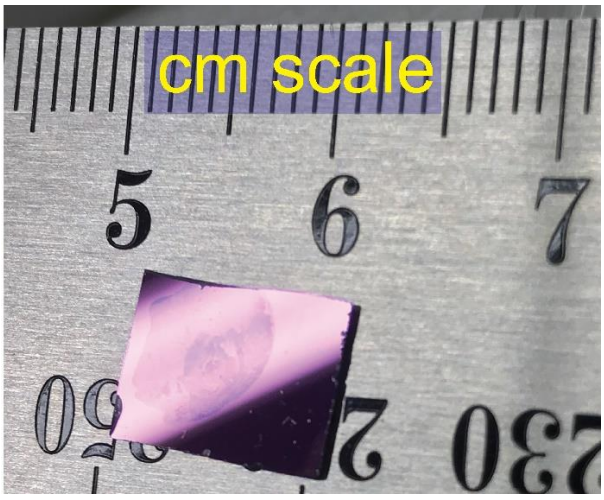

Figure S3. A representative 2D $In_2O_{3-x}S_x$ sheet printed on a SiO_2/Si substrate, approaching centimetre scale. It can be observed that the 2D sheet covers a homogeneous area of several millimetres with some inevitable folded regions at the edge and where the molten droplet was placed.

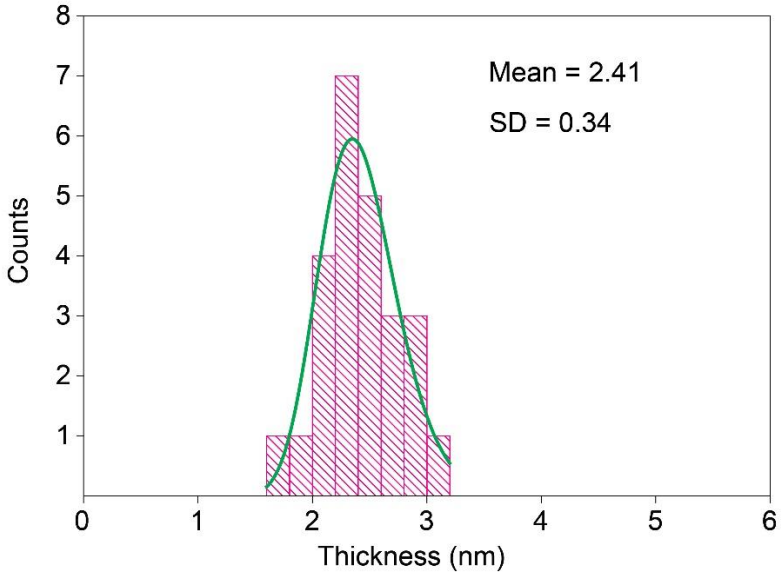

Figure S4. Statistical distribution of 2D $In_2O_{3-x}S_x$ sheets thickness. The mean and standard deviation (SD) were found to be 2.41 nm and 0.34 nm, respectively. The difference between measurements is due to AFM tip-surface interactions, noises from environment, and substrate effects.[3]

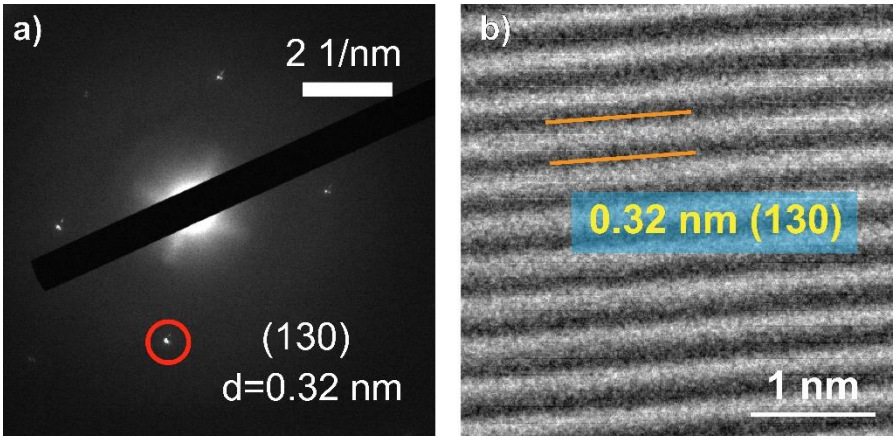

Figure S5. SAED pattern and HRTEM image of 2D In_2O_3 directly exfoliated from molten indium metal. The diffraction spot in red circle and a lattice spacing of 0.32 nm can be indexed to (130) plane of *c*-In_2O_3.[4] The crystal structure of cubic 2D In_2O_3 derived from liquid metal has been reported in the previous study.[5]

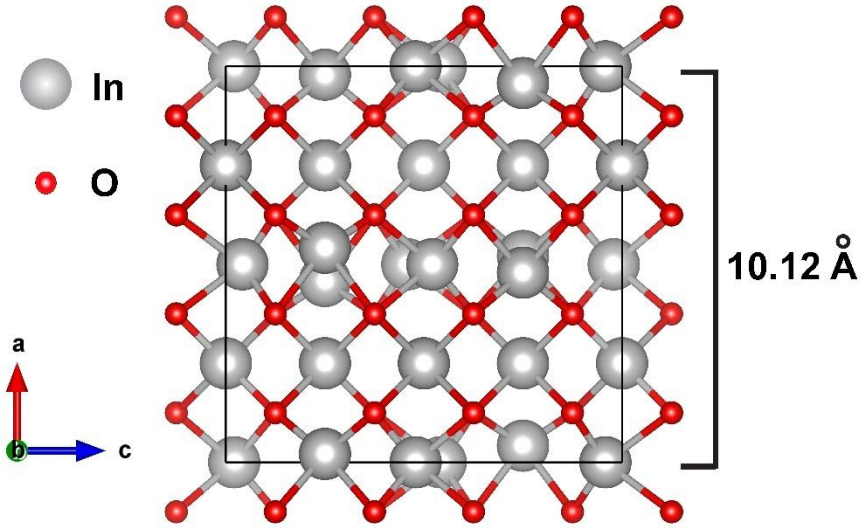

Figure S6. Crystal structure of *c*-In_2O_3 with the unit cell thickness of 10.12 Å.[4]

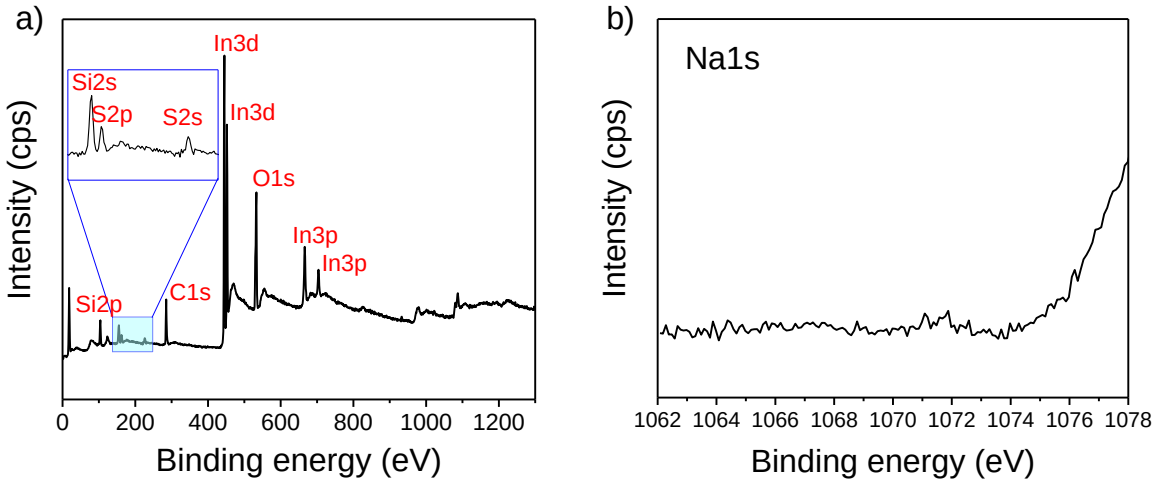

Figure S7. (a) XPS survey spectrum of 2D $In_2O_{3-x}S_x$ nanosheets. Si2*p* and Si2*s* peaks arising from the silicon substrate have been detected at 103.2 eV and 155.5 eV respectively. (b) High resolution XPS spectrum of Na 1*s* for 2D $In_2O_{3-x}S_x$ with no peaks being detected, indicating the absence of surface absorbed Na_2S.

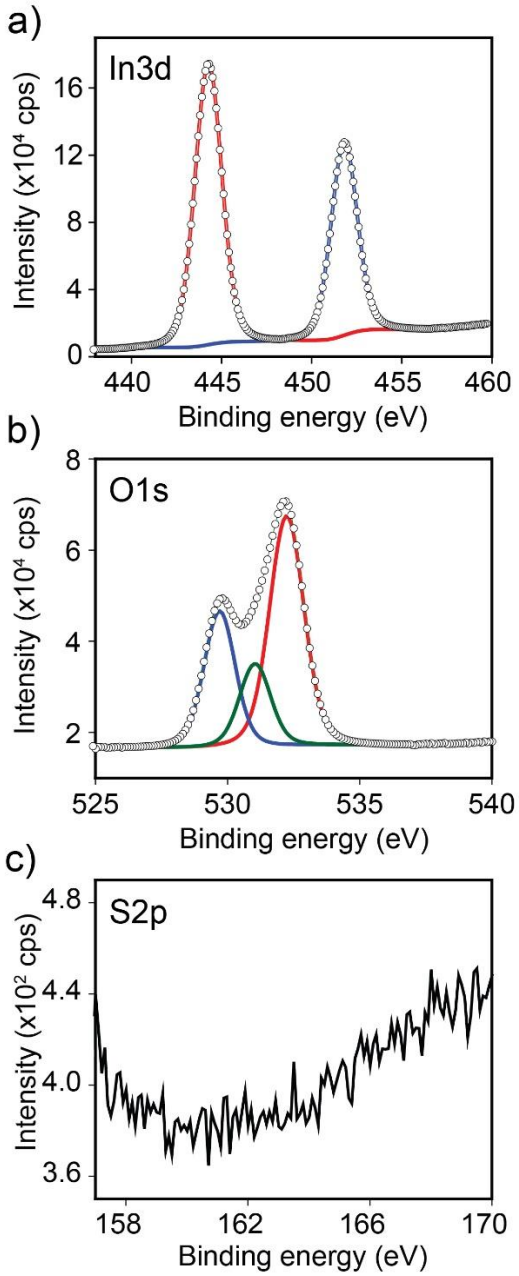

Figure S8. XPS spectra of 2D In_2O_3 nanosheets. (a) XPS scanning for In 3*d*: the doublet signal at 444.3 eV and 451.77 eV is associated with In $3d_{5/2}$ and In $3d_{3/2}$, respectively, no signals of indium metal have been recorded. (b) XPS scanning for O 1*s*: the dominant peak at 532.3 eV is related to Si-O-Si bonds in the substrate. The peak at 529.7 eV is attributed to O^{2-} ions in indium oxide lattice. The peak at 531.2 eV may be assigned to C=O bonds originating from surface contamination as well as oxygen atoms near defect sites. [6-11] (c) No peaks were detected in the S 2*p* region.

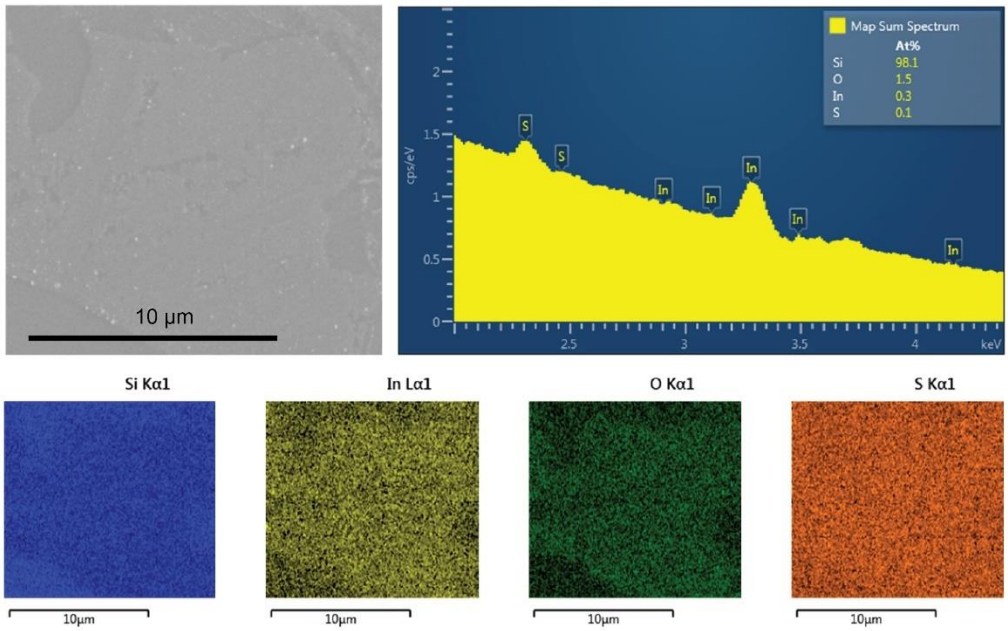

Figure S9. SEM-EDX spectrum of a 2D $In_2O_{3-x}S_x$ nanosheet prepared on 300 nm SiO_2/Si wafer with corresponding maps for the elements Si, In, O, and S. The analysis was conducted at a folded edge region that was thicker and hence provided better signal. The map sum spectrum reveals a In:S ratio of 3:1, with the signal being close to the detection limit. The excess oxygen is due to surface SiO_2 from the Si substrate. Because of the limitations of SEM-EDX, XPS elemental analysis is better suited and should be referred to when determining the composition of the synthesised nanosheets.

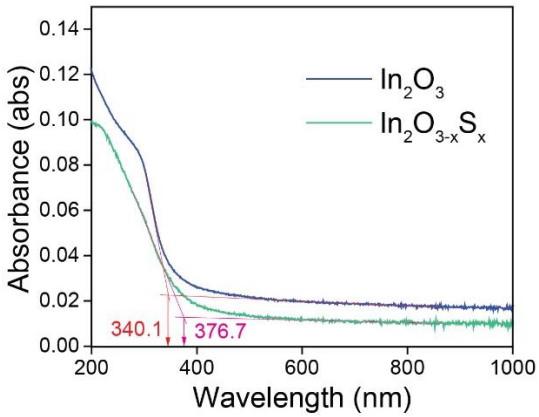

Figure S10. UV-vis spectra of 2D In_2O_3 and 2D $In_2O_{3-x}S_x$ (x=0.41) indicates the shift in light absorption from 340.1 nm to 376.7 nm.

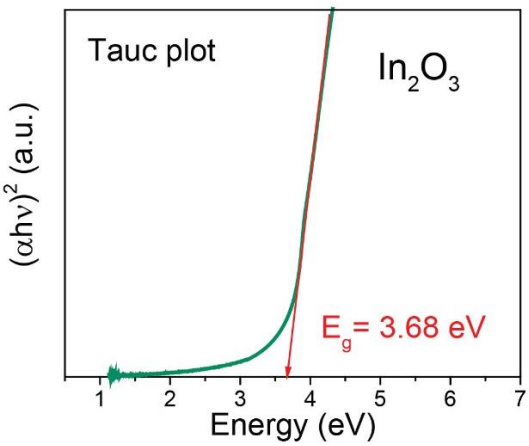

Figure S11. UV-vis Tauc plot of 2D In_2O_3 sample reveals a direct bandgap of 3.68 eV.

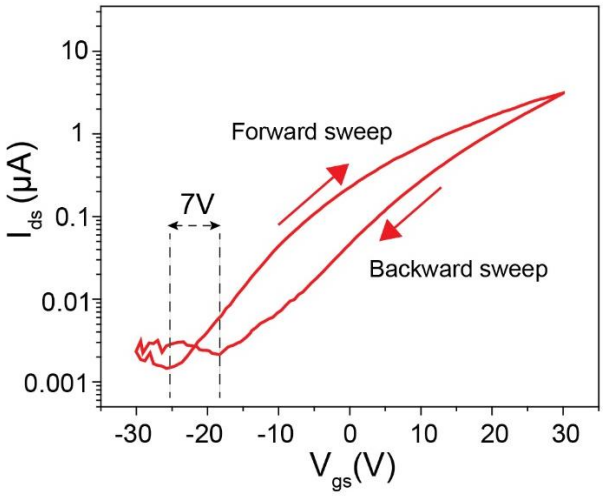

Figure S12. The transfer (I_{ds}-V_{gs}) curve with 1V source drain bias (V_{ds}) shown in a semi-logarithmic scale. The dashed black lines indicate the change in the position of the charge neutrality point. Red arrows indicate the back-gate sweep direction. The hysteresis can be assigned to the trapping and de-trapping of charge carriers by adsorbed water molecules or by trap states on the dielectric substrate.[12, 13]

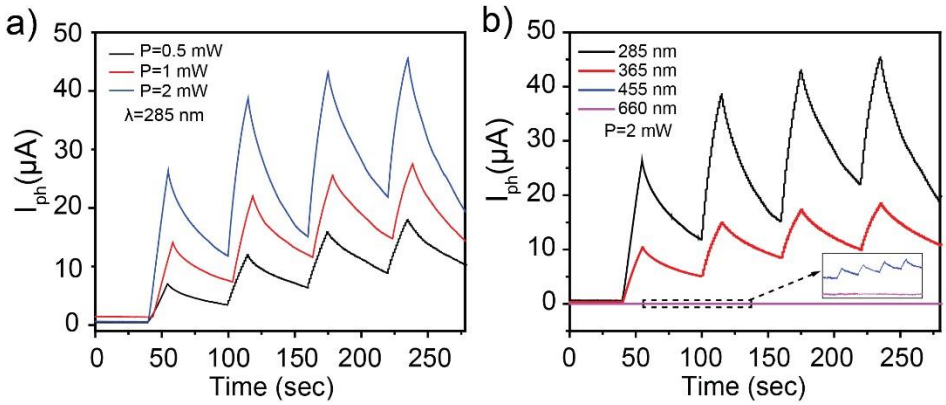

Figure S13. The photocurrent response of 2D $In_2O_{3-x}S_x$ based device as a function of time under (a) different applied powers of the incident light and (b) different wavelengths. The V_{ds} was set at 0.5 V.

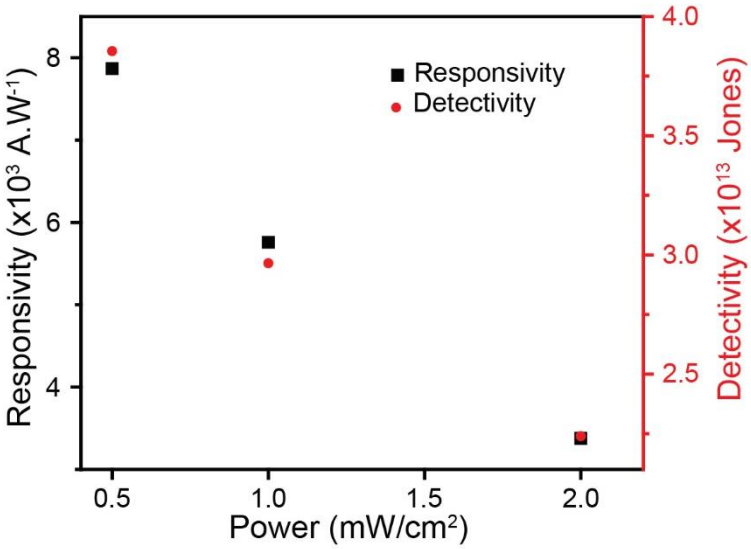

Figure S14. Responsivity and detectivity values of 2D $In_2O_{3-x}S_x$ based device at different power intensities, with the wavelength of 285 nm and 0.5 V bias voltage.

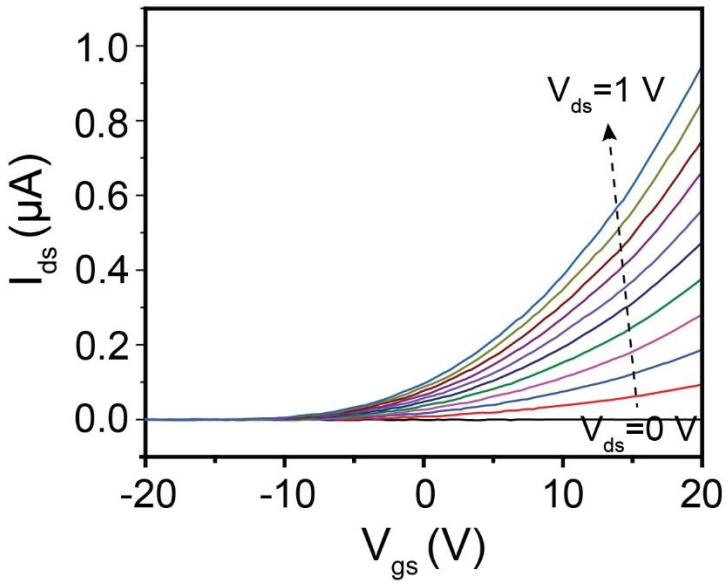

Figure S15. Transfer characteristic I_{ds}-V_{gs} of 2D In_2O_3 based device with V_{ds} being varied from 0 to 1 V.

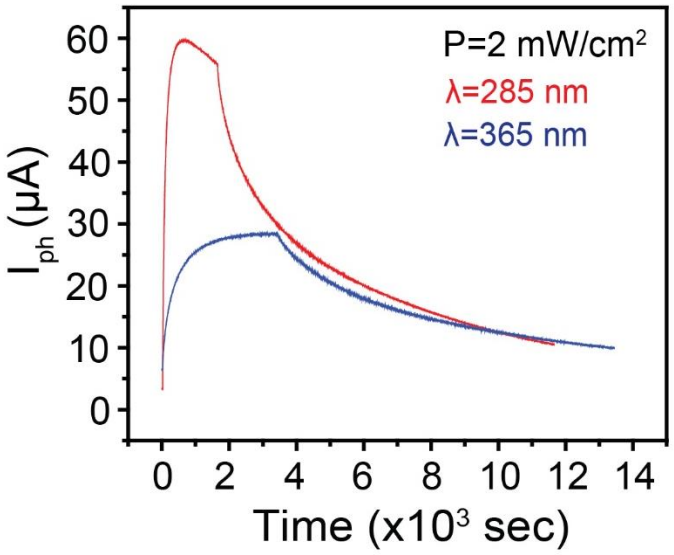

Figure S16. The photocurrent response of 2D In_2O_3 based photodetector under 285 nm and 365 nm UV exposure at P = 2 mW cm^{-2} and V_{ds} = 0.5 V. The device is more sensitive to shorter wavelengths and features a persistent photocurrent for several hours.

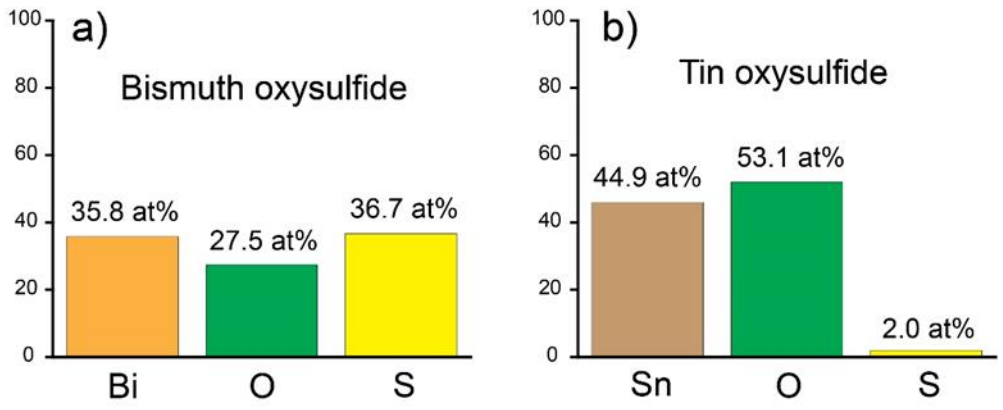

Figure S17. Elemental composition derived from XPS results of (a) 2D bismuth oxysulfide and (b) 2D tin oxysulfide.

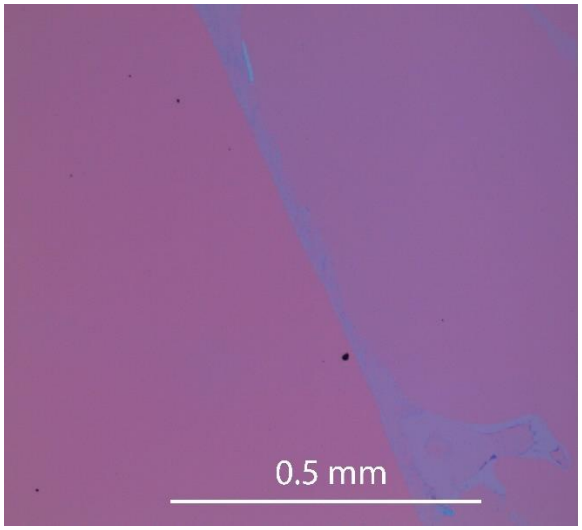

Figure S18. Optical image of an as-grown 2D In_2O_3 nanosheet on silicon substrate with a folded region being observed at the edge of the 2D sheet.

Table S1. Screening the reaction parameters for the transformation of 2D In_2O_3 into 2D $In_2O_{3-x}S_x$ (calculated from XPS data).

Sample	Temp. (°C)	Time (h)	S content (At%)	x
In_2O_3 as-synthesized *	-	-	0	0
In_2O_3 blank sample **	150	5	0	0
$In_2O_{3-x}S_x$	RT	5	<1	-
$In_2O_{3-x}S_x$	80	5	4.2	0.21
$In_2O_{3-x}S_x$	120	5	4.6	0.23
$In_2O_{3-x}S_x$ ***	150	5	8.3±0.5	0.41±0.02
$In_2O_{3-x}S_x$	200	5	7.8	0.39
$In_2O_{3-x}S_x$	150	1	<1	-
$In_2O_{3-x}S_x$	150	2	1.8	0.09
$In_2O_{3-x}S_x$	150	8	6.4	0.32

* 2D In_2O_3 was analysed after squeeze printing process

** 2D In_2O_3 was treated at optimized conditions, but without sulfur sources

*** Experiments have been repeated 4 times for standard error calculation

Note: x is calculated from the relation x=2/(In:S ratio) with In:S ratio being obtained from XPS data of 2D $In_2O_{3-x}S_x$. Sulfur content is calculated from the relation %S=100x/5

Table S2. Comparison of FETs based on 2D $In_2O_{3-x}S_x$ nanosheets with some reported 2D oxides and chalcogenides over the past few years.

Materials	Thickness (nm)	Method	Mobility ($cm^2V^{-1}s^{-1}$)	I_{On}/I_{Off}	Ref.
$In_2O_{3-x}S_x$	2.4	vdW Exfoliation and wet chemical process	44 * 20.4±6.3 **	0.6×10^2	This work
In_2O_3	2.0	vdW Exfoliation	5.5±1.5 **	4×10^2	This work
In_2O_3	1.5	vdW Exfoliation	4	10^5	[14]
In_2O_3	12-20	Inkjet-printing	3.98	10^8	[15]
SnO	0.4	vdW Exfoliation	0.7	20	[16]
SnO_2	50	Solution process and annealing	0.23	10^6	[17]
ZnO	5	ALD	2.8	10^5	[18]
IGZO	10	Solution process and annealing	9.1	10^6	[19]
In_2S_3	3.7	vdW Exfoliation and CVD	56	10^4	[1]
InSe	12	Mechanical exfoliation	0.1	10^4	[20]
InSe	41	Solvent exfoliation	19	10^6	[21]
α-Ga_2S_3	2	vdW Exfoliation and CVD	3.5	10^2	[22]
γ-Ga_2S_3	9	CVD	1.1	10^5	[23]
GaS	1.5	vdW Exfoliation and CVD	0.2	150	[24]
GaSe	1.1	Mechanical exfoliation	0.6	10^5	[25]
MoS_2	3	CVD	12.24	10^6	[26]
MoS_2	0.8	CVD	17	10^3	[27]
$MoSe_2$	3-80	Mechanical exfoliation	50	10^6	[28]
$MoTe_2$	1.6	Mechanical exfoliation	10	10^6	[29]
WS_2	0.7	CVD	0.91	10^6	[30]

*	Highest value
**	Average value with standard error

Table S3. Comparison of 2D $In_2O_{3-x}S_x$ nanosheets with other recently reported 2D nanosheets and commercial materials for photodetector performance. NM: not mentioned.

Materials	Wavelength (nm)	Thickness (nm)	R (A W^{-1})	D^* (Jones)	EQE (%)	Response time (ms)	Ref.
$In_2O_{3-x}S_x$	285	2.4	3.4×10^3	2.18×10^{13}	1.47×10^6	$t_{rise} = 42\times10^3$ $t_{fall} = 87\times10^3$	This work
$SnO\text{-}In_2O_3$	280	5.5	10^3	5×10^9	NM	≤1	[5]
Bi_2O_3	365	0.75	4×10^2	1.1×10^{13}	NM	0.07	[31]
Graphene-β-Ga_2O_3	254	2	1.48	2.24×10^{12}	7.27×10^2	3.1×10^5	[32]
γ-Ga_2S_3	350	9	61.3	1.52×10^{10}	2.17×10^4	10-15	[23]
GaS	254	2.3	4.2	10^{13}	2×10^3	<30	[33]
WS_2	365	25.2	53.3	1.22×10^{11}	NM	NM	[34]
MoS_2	405	1.3	6.3×10^{-5}	4.2×10^8	NM	20	[35]
InSe	254	30	5.6×10^4	2×10^{13}	NM	5	[36]
SnSe	370	9	5.5	6×10^{10}	1.83×10^3	NM	[37]
In_2Se_3	300	3.9	3.9×10^2	2.26×10^{12}	16.3×10^4	18	[38]
Commercial Si	400-1100	NM	0.5	3×10^{12}	NM	10^{-6}	[39]
Commercial GaP	150-550	NM	0.1	2×10^{13}	NM	1.1×10^{-4}	[39]

References

1. Jannat, A.; Yao, Q.; Zavabeti, A.; Syed, N.; Zhang, B. Y.; Ahmed, T.; Kuriakose, S.; Mohiuddin, M.; Pillai, N.; Haque, F.; Ren, G.; Zhu, D. M.; Cheng, N.; Du, Y.; Tawfik, S. A.; Spencer, M. J. S.; Murdoch, B. J.; Wang, L.; McConville, C. F.; Walia, S.; Daeneke, T.; Zhu, L.; Ou, J. Z., Ordered-vacancy-enabled indium sulphide printed in wafer-scale with enhanced electron mobility. *Mater. Horiz.* **2020,** *7* (3), 827-834.
2. Bugot, C.; Bouttemy, M.; Schneider, N.; Etcheberry, A.; Lincot, D.; Donsanti, F., New insights on the chemistry of plasma-enhanced atomic layer deposition of indium oxysulfide thin films and their use as buffer layers in Cu (In, Ga) Se2 thin film solar cell. *J. Vac. Sci. Technol., A* **2018,** *36* (6), 061510.
3. Marinello, F.; Carmignato, S.; Voltan, A.; Savio, E.; De Chiffre, L., Error Sources in Atomic Force Microscopy for Dimensional Measurements: Taxonomy and Modeling. *J. Manuf. Sci. Eng.* **2010,** *132* (3).
4. Marezio, M., Refinement of the crystal structure of In2O3 at two wavelengths. *Acta Crystallographica* **1966,** *20* (6), 723-728.
5. Alsaif, M. M. Y. A.; Kuriakose, S.; Walia, S.; Syed, N.; Jannat, A.; Zhang, B. Y.; Haque, F.; Mohiuddin, M.; Alkathiri, T.; Pillai, N.; Daeneke, T.; Ou, J. Z.; Zavabeti, A., 2D SnO/In2O3 van der Waals Heterostructure Photodetector Based on Printed Oxide Skin of Liquid Metals. *Advanced Materials Interfaces* **2019,** *6* (7), 1900007.

6. Beena, D.; Lethy, K. J.; Vinodkumar, R.; Mahadevan Pillai, V. P.; Ganesan, V.; Phase, D. M.; Sudheer, S. K., Effect of substrate temperature on structural, optical and electrical properties of pulsed laser ablated nanostructured indium oxide films. *Appl. Surf. Sci.* **2009,** *255* (20), 8334-8342.
7. Gan, J.; Lu, X.; Wu, J.; Xie, S.; Zhai, T.; Yu, M.; Zhang, Z.; Mao, Y.; Wang, S. C. I.; Shen, Y., Oxygen vacancies promoting photoelectrochemical performance of In 2 O 3 nanocubes. *Scientific reports* **2013,** *3* (1), 1-7.
8. Kim, J.; Ho, P.; Thomas, D.; Friend, R.; Cacialli, F.; Bao, G.-W.; Li, S., X-ray photoelectron spectroscopy of surface-treated indium-tin oxide thin films. *Chem. Phys. Lett.* **1999,** *315* (5-6), 307-312.
9. Donley, C.; Dunphy, D.; Paine, D.; Carter, C.; Nebesny, K.; Lee, P.; Alloway, D.; Armstrong, N. R., Characterization of Indium− Tin oxide interfaces using X-ray photoelectron spectroscopy and redox processes of a chemisorbed probe molecule: effect of surface pretreatment conditions. *Langmuir* **2002,** *18* (2), 450-457.
10. Fan, J. C.; Goodenough, J. B., X-ray photoemission spectroscopy studies of Sn-doped indium-oxide films. *J. Appl. Phys.* **1977,** *48* (8), 3524-3531.
11. Schneuwly, A.; Gröning, P.; Schlapbach, L.; Jaecklin, V. P., Influence of surface contamination on metal/metal bond contact quality. *J. Electron. Mater.* **1998,** *27* (8), 990-997.
12. Shu, J.; Wu, G.; Guo, Y.; Liu, B.; Wei, X.; Chen, Q., The intrinsic origin of hysteresis in MoS 2 field effect transistors. *Nanoscale* **2016,** *8* (5), 3049-3056.
13. Kathalingam, A.; Senthilkumar, V.; Rhee, J.-K., Hysteresis I–V nature of mechanically exfoliated graphene FET. *J. Mater. Sci.: Mater. Electron.* **2014,** *25* (3), 1303-1308.
14. Jannat, A.; Syed, N.; Xu, K.; Rahman, M. A.; Talukder, M. M. M.; Messalea, K. A.; Mohiuddin, M.; Datta, R. S.; Khan, M. W.; Alkathiri, T.; Murdoch, B. J.; Reza, S. Z.; Li, J.; Daeneke, T.; Zavabeti, A.; Ou, J. Z., Printable Single-Unit-Cell-Thick Transparent Zinc-Doped Indium Oxides with Efficient Electron Transport Properties. *ACS Nano* **2021**.
15. Lee, J. S.; Kwack, Y.-J.; Choi, W.-S., Inkjet-Printed In2O3 Thin-Film Transistor below 200 °C. *ACS Appl. Mater. Interfaces* **2013,** *5* (22), 11578-11583.
16. Daeneke, T.; Atkin, P.; Orrell-Trigg, R.; Zavabeti, A.; Ahmed, T.; Walia, S.; Liu, M.; Tachibana, Y.; Javaid, M.; Greentree, A. D.; Russo, S. P.; Kaner, R. B.; Kalantar-Zadeh, K., Wafer-Scale Synthesis of Semiconducting SnO Monolayers from Interfacial Oxide Layers of Metallic Liquid Tin. *ACS Nano* **2017,** *11* (11), 10974-10983.
17. D.M, P.; Mannam, R.; Rao, M. S. R.; DasGupta, N., Effect of annealing ambient on SnO2 thin film transistors. *Appl. Surf. Sci.* **2017,** *418*, 414-417.
18. Yoon, M.; Park, J.; Tran, D. C.; Sung, M. M., Fermi-Level Engineering of Atomic Layer-Deposited Zinc Oxide Thin Films for a Vertically Stacked Inverter. *ACS Appl. Electron. Mater.* **2020,** *2* (2), 537-544.
19. Xu, W.; Hu, L.; Zhao, C.; Zhang, L.; Zhu, D.; Cao, P.; Liu, W.; Han, S.; Liu, X.; Jia, F.; Zeng, Y.; Lu, Y., Low temperature solution-processed IGZO thin-film transistors. *Appl. Surf. Sci.* **2018,** *455*, 554-560.
20. Tamalampudi, S. R.; Lu, Y.-Y.; U, R. K.; Sankar, R.; Liao, C.-D.; B, K. M.; Cheng, C.-H.; Chou, F. C.; Chen, Y.-T., High Performance and Bendable Few-Layered InSe Photodetectors with Broad Spectral Response. *Nano Lett.* **2014,** *14* (5), 2800-2806.
21. Kang, J.; Wells, S. A.; Sangwan, V. K.; Lam, D.; Liu, X.; Luxa, J.; Sofer, Z.; Hersam, M. C., Solution-Based Processing of Optoelectronically Active Indium Selenide. *Adv. Mater.* **2018,** *30* (38), 1802990.
22. Alsaif, M. M. Y. A.; Pillai, N.; Kuriakose, S.; Walia, S.; Jannat, A.; Xu, K.; Alkathiri, T.; Mohiuddin, M.; Daeneke, T.; Kalantar-Zadeh, K.; Ou, J. Z.; Zavabeti, A., Atomically Thin Ga2S3 from Skin of Liquid Metals for Electrical, Optical, and Sensing Applications. *ACS Appl. Nano Mater.* **2019,** *2* (7), 4665-4672.

23. Zhou, N.; Gan, L.; Yang, R.; Wang, F.; Li, L.; Chen, Y.; Li, D.; Zhai, T., Nonlayered Two-Dimensional Defective Semiconductor γ-Ga2S3 toward Broadband Photodetection. *ACS Nano* **2019,** *13* (6), 6297-6307.
24. Carey, B. J.; Ou, J. Z.; Clark, R. M.; Berean, K. J.; Zavabeti, A.; Chesman, A. S. R.; Russo, S. P.; Lau, D. W. M.; Xu, Z.-Q.; Bao, Q.; Kavehei, O.; Gibson, B. C.; Dickey, M. D.; Kaner, R. B.; Daeneke, T.; Kalantar-Zadeh, K., Wafer-scale two-dimensional semiconductors from printed oxide skin of liquid metals. *Nat. Commun.* **2017,** *8* (1), 14482.
25. Late, D. J.; Liu, B.; Luo, J.; Yan, A.; Matte, H. S. S. R.; Grayson, M.; Rao, C. N. R.; Dravid, V. P., GaS and GaSe Ultrathin Layer Transistors. *Adv. Mater.* **2012,** *24* (26), 3549-3554.
26. Park, J.; Choudhary, N.; Smith, J.; Lee, G.; Kim, M.; Choi, W., Thickness modulated MoS2 grown by chemical vapor deposition for transparent and flexible electronic devices. *Appl. Phys. Lett.* **2015,** *106* (1), 012104.
27. Yu, L.; Lee, Y.-H.; Ling, X.; Santos, E. J. G.; Shin, Y. C.; Lin, Y.; Dubey, M.; Kaxiras, E.; Kong, J.; Wang, H.; Palacios, T., Graphene/MoS2 Hybrid Technology for Large-Scale Two-Dimensional Electronics. *Nano Lett.* **2014,** *14* (6), 3055-3063.
28. Larentis, S.; Fallahazad, B.; Tutuc, E., Field-effect transistors and intrinsic mobility in ultra-thin MoSe2 layers. *Appl. Phys. Lett.* **2012,** *101* (22), 223104.
29. Pradhan, N. R.; Rhodes, D.; Feng, S.; Xin, Y.; Memaran, S.; Moon, B.-H.; Terrones, H.; Terrones, M.; Balicas, L., Field-Effect Transistors Based on Few-Layered α-MoTe2. *ACS Nano* **2014,** *8* (6), 5911-5920.
30. Lan, C.; Li, C.; Yin, Y.; Liu, Y., Large-area synthesis of monolayer WS2 and its ambient-sensitive photo-detecting performance. *Nanoscale* **2015,** *7* (14), 5974-5980.
31. Messalea, K. A.; Carey, B. J.; Jannat, A.; Syed, N.; Mohiuddin, M.; Zhang, B. Y.; Zavabeti, A.; Ahmed, T.; Mahmood, N.; Della Gaspera, E.; Khoshmanesh, K.; Kalantar-Zadeh, K.; Daeneke, T., Bi2O3 monolayers from elemental liquid bismuth. *Nanoscale* **2018,** *10* (33), 15615-15623.
32. Kong, W.-Y.; Wu, G.-A.; Wang, K.-Y.; Zhang, T.-F.; Zou, Y.-F.; Wang, D.-D.; Luo, L.-B., Graphene-β-Ga2O3 Heterojunction for Highly Sensitive Deep UV Photodetector Application. *Adv. Mater.* **2016,** *28* (48), 10725-10731.
33. Hu, P.; Wang, L.; Yoon, M.; Zhang, J.; Feng, W.; Wang, X.; Wen, Z.; Idrobo, J. C.; Miyamoto, Y.; Geohegan, D. B.; Xiao, K., Highly Responsive Ultrathin GaS Nanosheet Photodetectors on Rigid and Flexible Substrates. *Nano Lett.* **2013,** *13* (4), 1649-1654.
34. Zeng, L.; Tao, L.; Tang, C.; Zhou, B.; Long, H.; Chai, Y.; Lau, S. P.; Tsang, Y. H., High-responsivity UV-Vis Photodetector Based on Transferable WS2 Film Deposited by Magnetron Sputtering. *Sci. Rep* **2016,** *6* (1), 20343.
35. Lee, Y.; Yang, J.; Lee, D.; Kim, Y.-H.; Park, J.-H.; Kim, H.; Cho, J. H., Trap-induced photoresponse of solution-synthesized MoS2. *Nanoscale* **2016,** *8* (17), 9193-9200.
36. Feng, W.; Wu, J.-B.; Li, X.; Zheng, W.; Zhou, X.; Xiao, K.; Cao, W.; Yang, B.; Idrobo, J.-C.; Basile, L.; Tian, W.; Tan, P.; Hu, P., Ultrahigh photo-responsivity and detectivity in multilayer InSe nanosheets phototransistors with broadband response. *J. Mater. Chem. C* **2015,** *3* (27), 7022-7028.
37. Yao, J.; Zheng, Z.; Yang, G., All-Layered 2D Optoelectronics: A High-Performance UV–vis–NIR Broadband SnSe Photodetector with Bi2Te3 Topological Insulator Electrodes. *Adv. Funct. Mater.* **2017,** *27* (33), 1701823.
38. Jacobs-Gedrim, R. B.; Shanmugam, M.; Jain, N.; Durcan, C. A.; Murphy, M. T.; Murray, T. M.; Matyi, R. J.; Moore, R. L.; Yu, B., Extraordinary Photoresponse in Two-Dimensional In2Se3 Nanosheets. *ACS Nano* **2014,** *8* (1), 514-521.
39. Krishnamurthi, V.; Khan, H.; Ahmed, T.; Zavabeti, A.; Tawfik, S. A.; Jain, S. K.; Spencer, M. J. S.; Balendhran, S.; Crozier, K. B.; Li, Z.; Fu, L.; Mohiuddin, M.; Low, M. X.; Shabbir, B.; Boes, A.; Mitchell, A.; McConville, C. F.; Li, Y.; Kalantar-Zadeh, K.; Mahmood, N.; Walia, S., Liquid-Metal Synthesized Ultrathin SnS Layers for High-Performance Broadband Photodetectors. *Adv. Mater.* **2020,** *32* (45), 2004247.